Low intensity 635 nm diode laser irradiation inhibits fibroblast-myofibroblast transition reducing TRPC1 channel expression/activity:

Lasers in Surgery and Medicine

LOW INTENSITY 635 nm DIODE LASER IRRADIATION INHIBITS FIBROBLAST-MYOFIBROBLAST TRANSITION REDUCING TRPC1 CHANNEL EXPRESSION/ACTIVITY: NEW PERSPECTIVES FOR TISSUE FIBROSIS TREATMENT

Journal:	*Lasers in Surgery & Medicine*
Manuscript ID	LSM-15-0221.R1
Wiley - Manuscript type:	Basic Science
Date Submitted by the Author:	n/a
Complete List of Authors:	Sassoli, Chiara; University Of Florence; Florence , Italy, Experimental and Clinical Medicine Chellini, Flaminia; University of Florence, Experimental and Clinical Medicine-Section of Anatomy and Histology Squecco, Roberta; University of Florence, Experimental and Clinical Medicine -Section of Physiological Sciences Tani, Alessia; University of Florence, Experimental and Clinical Medicine-Section of Anatomy and Histology Idrizaj, Eglantina; University of Florence, Experimental and Clinical Medicine -Section of Physiological Sciences Nosi, Daniele; University of Florence, Experimental and Clinical Medicine-Section of Anatomy and Histology Giannelli, Marco; Odontostomatologic Laser Therapy Center Zecchi-Orlandini, Sandra; University of Florence, Experimental and Clinical Medicine-Section of Anatomy and Histology
Key Words:	alfa-sma, Low Level Laser Therapy (LLLT), matrix metalloproteases (MMPs), stress fibers, stretch activated channel (SAC), Transforming Growth Factor (TGF)-beta1, Tissue Inhibitor of metalloprotease (TIMP), Type-1 collagen, photobiomodulation

LOW INTENSITY 635 nm DIODE LASER IRRADIATION INHIBITS FIBROBLAST-MYOFIBROBLAST TRANSITION REDUCING TRPC1 CHANNEL EXPRESSION/ACTIVITY: NEW PERSPECTIVES FOR TISSUE FIBROSIS TREATMENT

Chiara Sassoli, BSc, PhD[1*], Flaminia Chellini, BSc, PhD[1], Roberta Squecco, BSc, PhD[2], Alessia Tani, BSc, PhD[1], Eglantina Idrizaj, PharmD[2], Daniele Nosi, BSc, PhD[1], Marco Giannelli, MD[3], Sandra Zecchi-Orlandini, BSc[1]

[1]Department of Experimental and Clinical Medicine - Section of Anatomy and Histology, Largo Brambilla 3, University of Florence, 50134 Florence, Italy (CS, FC, AT, DN, SZO)

[2]Department of Experimental and Clinical Medicine -Section of Physiological Sciences, Viale GB Morgagni 63, University of Florence, 50134 Florence, Italy (RS, EI)

[3]Odontostomatologic Laser Therapy Center, Via dell' Olivuzzo 162, 50143, Florence, Italy (MG)

Acknowledgements and Grants: This study was supported by Odontostomatologic Laser Therapy Center and by project research founds from MIUR (Ministero dell'Istruzione dell'Università e della Ricerca)- Italy to CS, RS, DN, SZO.

***Correspondence to:**

Dr. Chiara Sassoli
Department of Experimental and Clinical Medicine - Section of Anatomy and Histology
University of Florence
Largo Brambilla 3, 50134 Florence, Italy
Tel +39 552758063
Fax +39 554379500
E-mail chiara.sassoli@unifi.it

Key words: α-sma; Low Level Laser Therapy (LLLT); matrix metalloproteases (MMPs); photobiomodulation; stress fibers; stretch activated channel (SAC); Transforming Growth Factor (TGF)-β1; Tissue Inhibitor of metalloprotease (TIMP); Type-1 collagen.

ABSTRACT

BACKGROUND AND OBJECTIVE: Low Level Laser Therapy (LLLT) or photobiomodulation therapy is emerging as a promising new therapeutic option for fibrosis in different damaged and/or diseased organs. However, the anti-fibrotic potential of this treatment needs to be elucidated and the cellular and molecular targets of the laser clarified. Here we investigated the effects of a low intensity 635±5 nm diode laser irradiation on fibroblast-myofibroblast transition, a key event in the onset of fibrosis, and elucidated some of the underlying molecular mechanisms.

MATERIALS AND METHODS: NIH/3T3 fibroblasts were cultured in a low serum medium in the presence of Transforming Growth Factor (TGF)-β1, irradiated with a 635±5 nm diode laser (continuous wave, 89 mW, 0.3 J/cm^2). Fibroblast-myofibroblast differentiation was assayed by morphological, biochemical and electrophysiological approaches. Expression of matrix metalloproteinase (MMP)-2 and MMP-9 and of Tissue inhibitor of MMPs, namely TIMP-1 and TIMP-2, after laser exposure were also evaluated by confocal immunofluorescence analyses. Moreover, the effect of the diode laser on Transient Receptor Potential Canonical Channel (TRPC)1/Stretch Activated Channel (SAC) expression and activity and on TGF-β1/Smad3 signaling was investigated.

RESULTS: Diode laser treatment inhibited TGF-β1-induced fibroblast-myofibroblast transition as judged by reduction of stress fibers formation, α–smooth muscle actin (sma) and type-1 collagen expression and by changes in electrophysiological properties such as resting membrane potential, cell capacitance and inwardly rectifying K^+ currents. In addition, the irradiation up-regulated the expression of MMP-2 and MMP-9 and downregulated that of TIMP-1 and TIMP-2 in TGF-β1-treated cells. This laser effect was shown to involve TRPC1/SAC channel functionality. Finally, diode laser stimulation and TRPC1 functionality negatively affected fibroblast-myofibroblast transition by interfering with TGF-β1 signaling, namely reducing the expression of Smad3, the TGF-β1 downstream signaling molecule.

CONCLUSION: Low intensity irradiation with 635±5 nm diode laser inhibited TGF-β1/Smad3-mediated fibroblast-myofibroblast transition and this effect involved the modulation of TRPC1 ion channels. These data contribute to support the potential anti-fibrotic effect of LLLT and may offer further informations for considering this therapy as a promising therapeutic tool for the treatment of tissue fibrosis.

INTRODUCTION

Fibrosis represents a process influencing both progression and outcome of several diseases and it is estimated that, in developed countries, 45% of deaths can be attributed to pathologies where fibrosis plays a major aetiological role [1,2]. Fibrosis frequently occurs as aberrant response to an injury or chronic diseases, leading to the impairment of the functionality of multiple organs including heart, skeletal muscle, liver, kidney, lung and skin [3-8]. Also reactive stroma of solid tumors can be considered as a fibrotic tissue [9] and, in addition, the oral sub-mucosal layer may be affected by fibrosis as well, for instance after direct exposure of the buccal mucosa to noxious chemicals and additives with severe consequences for periodontal tissue [10].

In all cases, fibrosis consists of an excessive extracellular matrix (ECM) deposition attributable to the imbalance between collagen synthesis and degradation, in turn depending on the expression of collagen-related genes and activity of matrix metalloproteinases (MMPs) and their inhibitors (Tissue inhibitor of MMPs - TIMPs) [11]. The main cell type implicated in the onset and progression of fibrosis is the myofibroblast resulting from the activation and differentiation of fibroblasts [12]. Although myofibroblasts are required for the wound healing process and the reparative response to organ/tissue damage, their persistence in the damage site contributes to the excessive accumulation of ECM components, which ultimately replaces the necrotic or damaged tissue with a fibrotic scar. The current therapeutic options for fibrosis are very limited and at present, organ transplantation, when possible, is the only effective treatment for end-stage disease. Therefore, the development of alternative and effective therapies aimed to limit fibrotic response or even reverse the fibrotic pattern represents an urgent need with a potentially high impact on social wealth.

Along this line, much attention has been given in the recent years to molecules with anti-fibrotic effects [13-15]. In this context, studies conducted by our group and others have shown that the hormone relaxin can contribute to counteract fibrosis, inhibiting myofibroblast differentiation and modulating the expression of MMPs [16-19]. Moreover, emerging evidence suggests that cell-based therapy, utilizing mesenchymal stromal cells and other cell types, could attenuate the fibrogenic response in different tissues [19-22]. However, both the pharmacological and the cell-based approach present several criticisms and side effects which limit their clinical application. Indeed, soluble factors are typically short-lived, thus requiring more effective methods of delivery. On the other hand, the limitations of cell therapy are mainly related with the route of cell delivery in the host tissue which is still an issue of debate, the transient survival of the majority of transplanted cells within the recipient tissue and to the fact that long-term studies are required to elucidate the real outcome, side-effects and to validate the safety of transplanted cells.

A promising alternative therapeutic tool for the treatment of fibrosis could be represented by the Low Level Laser Therapy (LLLT) or photobiomodulation therapy. This approach consists in the direct application of a non ionizing light, usually delivered via a low power coherent light (laser) or non-coherent light sources such as filtered lamps or light-emitting diode (LED), typically emitting in the 600–1000 nm spectrum range (red to near infrared), with an energy density < 100 J/cm^2. Given the low energy density and wavelengths used in this therapy, light is able to easily enter the tissues in a non destructive and non thermal mode resulting in the biomodulation of various cellular processes [23-27].

LLLT is considered a safe technology and is widely applied in different branches of medicine and dentistry for pain management, to promote coagulation and reduce inflammation with satisfactory outcomes [27-29]. Moreover, many studies show the beneficial effects of the photobiomodulation therapy on healing and repair/regeneration processes at different tissues [30-37]. Along this line, we have recently demonstrated that therapy with different types of diode lasers is able to improve healing in chronic periodontitis patients [38]. More recently, photobiomodulation therapy is reported to have beneficial effects in reducing fibrosis in different damaged and/or diseased organs [27,28,33,39-45]. However despite these promising data, the anti-fibrotic potential of this kind of laser therapy needs to be further investigated and confirmed prior to clinical use as new treatment option for fibrosis. Indeed, the complexity of medical lasers in terms of different wavelengths, energy output modes and setting parameters has produced a multiplicity of protocols with different outcomes, thus sometimes hampering comparison of the results and identification of univocal guidelines for their use; moreover, although the remarkable increase of data concerning the mechanisms underlying the anti-fibrotic effect of photobiomodulation in recent years, the cellular and molecular targets of the laser treatment are far from being elucidated.

On the basis of these considerations, the aim of the present study was to further extend the knowledge on the anti-fibrotic action of photobiomodulation by examining the effect of low energy diode laser (635±5 nm) irradiation on the *in vitro* transition of NIH/3T3 fibroblasts into myofibroblasts and investigating the underlying molecular mechanisms.

MATERIALS AND METHODS

Cell culture and treatments

Murine fibroblasts NIH/3T3 cells obtained from ATCC were cultured in Dulbecco's modified Eagle's medium (DMEM; Sigma, Milan, Italy) with 4.5 g/l glucose, supplemented with 10% fetal bovine serum (FBS; Sigma), 1% penicillin/streptomycin (Sigma) at 37°C in a humidified

atmosphere of 5% CO_2. The cells were induced to differentiate into myofibroblasts by culturing in DMEM containing FBS 2% for 24 h, 48 h and 72 h in the presence of human Transforming Growth Factor (TGF)-β1 (2 ng/ml; PeproTech, Inc., Rocky Hill, NJ, USA) according to our previous work [16] and irradiated or not with diode laser. In some experiments the cells were also treated with Gadolinium Chloride ($GdCl_3$; 50 µM; Sigma) a commonly used pharmacological Stretch Activated Channel (SAC) blocker [24], prior laser irradiation.

Laser treatment

Irradiation was carried out with a diode laser (4x4 ™ Dental Laser System, General Project, Montespertoli, Florence, Italy) operating at a wavelength of 635±5 nm in continuous irradiation mode. The beam power was set at 89 mW and a 600 nm diameter optic fiber was used. The detailed laser specification and irradiation parameters were reported in Table 1. During the treatment, the temperature of the diode laser-irradiated cells was monitored by a thermal probe included in the console of the 4x4™ Dental Laser System and a thermal camera (Ti9, Fluke Corp., Everett, USA) able to show a thermal map of the treated area. This information allowed to finely tune the diode laser irradiation and keep the temperature below the cell damage threshold. To avoid overlapping or scattered irradiation, the cells of each cell preparation and experiment were seeded in wells or dishes spaced apart. A black background in the irradiation area was used to minimize light reflection. During the period of diode laser irradiation, the cover plate was removed and all the procedures were performed under ‘‘clean bench’’ conditions to prevent bacterial contamination. Eye protection of the operator and assistant was assured by wearing safety glasses.

MTS cell viability assay

Cell viability was determined by 3-(4.5-dimethylthiazol-2-yl)-5-(3-carboxymethoxyphenyl)-2-(4-sulfophenyl)-2Htetrazolium (MTS) assay (Promega Corp., Madison, WI, USA), essentially as previously reported [25]. Briefly, the cells were cultured in 96-well plates (6 x 10^3 cells/well) in DMEM supplemented with FBS 10% (control) and, after 24 h, were transferred in low serum (FBS 2%) phenol red-free culture medium in the presence of 2 ng/ml human TGF-β1, diode laser irradiated for 10 s as indicated in Table 1 (*treated surface diameter: 18 mm*) or not, and cultured for 24 h. Then the cells were transferred in 100 µl of fresh medium and 20 µl of MTS test solution was added to each well. After 4 h of incubation, the optical density (OD) of soluble formazan was measured using a multi-well scanning spectrophotometer (ELISA reader; Amersham, Pharmacia Biotech, Cambridge, UK) at a wavelength of 492 nm.

Silencing of TRPC1 by siRNA

To inhibit the expression of TRPC1, a mix of short interfering RNA duplexes (siRNA) (Santa Cruz Biotechnology, Santa Cruz, CA, USA) corresponding to three distinct regions of the DNA sequence of mouse TRPC1 gene (NM_011643) was used essentialy as previously reported [46]. A non-specific scrambled (SCR)-siRNA (Santa Cruz Biotechnology) was used as control. NIH/3T3 fibroblasts at 80% confluence were transfected using siRNA Transfection Reagent according to manifacturer's instructions (Santa Cruz Biotechnology) with TRPC1-siRNA duplexes or with SCR-siRNA (20 nM) for 24 h and then transferred in fresh medium for additional 5 h. After that the cells were cultured for further 24 h in low serum culture medium (FBS 2%) in the presence of 2 ng/ml TGF-β1 and irradiated with diode laser for 26 sec as indicated in the Table 1 (*treated surface diameter: 30 mm*) or not before being collected and processed for Western blotting analisys or fixed for confocal immunofluorescence staining. The specific knock-down of TRPC1 was evaluated by Western blotting (data not shown) and confocal immunofluorescence analysis. The efficiency of transfection was estimated to range from 70 to 80%.

Confocal Immunofluorescence

The cells grown on glass coverslips, were fixed with 0.5% buffered paraformaldehyde (PFA) for 10 min at room temperature (RT). After permeabilization with cold acetone for 3 min, the fixed cells were blocked with 0.5% bovine serum albumin (BSA; Sigma) and 3% glycerol in PBS for 20 min and then incubated overnight at 4°C, with the following primary antibodies: rabbit polyclonal anti-Ki67 (1:100; Santa Cruz Biotechnology), rabbit polyclonal anti-MMP-2 (1:200; Abcam, Cambridge, UK), rabbit polyclonal anti-MMP-9 (1.100; Abcam), rabbit polyclonal anti-TIMP-1 (1:50; Bioss Inc, Woburn, MA, USA), mouse monoclonal anti-TIMP-2 (1:20; Abcam), rabbit polyclonal anti-type-1 collagen (1:50; Santa Cruz Biotechnology), mouse monoclonal anti-alfa smooth muscle actin (α-sma, 1:100; Abcam), rabbit polyclonal anti-TRPC1 (1:80; Santa Cruz Biotechnology). The immunoreactions were revealed by incubation with specific anti-rabbit or anti-mouse Alexa Fluor 488- or 568-conjugated IgG (1:200; Molecular Probes, Eugene, OR, USA) for 1 h at RT. In some experiments, the cells were stained with Tetramethylrhodamine isothiocyanate (TRITC)-labeled phalloidin (1:100; Sigma) to reveal actin filament organization. In others experiments counterstaining was performed with propidium iodide (PI, 1:30; Molecular Probes) to reveal nuclei. Negative controls were carried out by replacing the primary antibodies with non immune serum; cross-reactivity of the secondary antibodies was tested in control experiments in which primary antibodies were omitted. After washing, the coverslips containing the immunolabelled cells were mounted with an antifade mounting medium (Biomeda Gel mount, Electron Microscopy Sciences, Foster City, CA, USA) and observed under a confocal Leica TCS

SP5 microscope (Leica Microsystems, Mannheim, Germany) equipped with a HeNe/Ar laser source for fluorescence measurements. Observations were performed using a Leica Plan Apo 63X/1.43NA oil immersion objective. Series of optical sections (1024 x 1024 pixels each; pixel size 204.3 nm) 0.4 µm in thickness were taken through the depth of the cells at intervals of 0.4 µm. Images were then projected onto a single 'extended focus' image. Densitometric analyses of the intensity of MMP-2, MMP-9, TIMP-1, TIMP-2, type-1 collagen, α-sma, TRPC1 fluorescent signals were performed on digitized images using ImageJ software (http://rsbweb.nih.gov/ij) in 20 regions of interest (ROI) of 100 µm2 for each confocal stacks (at least 10).

The number of NIH/3T3 cells with Ki67 positive nuclei was evaluated in 10 random 200 x 200 µm square microscopic fields (63X ocular) in each cell preparation and expressed as percentage of the total cell number.

Western Blotting

Cells were resuspended in appropriate volume of cold Cell Extraction Buffer (10 mM Tris/HCl, pH 7.4, 100 mM NaCl, 1 mM EDTA, 1 mM EGTA, 1 mM NaF, 20 mM Na4P2O7, 2 mM Na3VO4, 1% Triton X-100, 10% glycerol, 0.1% SDS, 0.5% deoxycholate; Invitrogen Life Technologies, Grand Island, NY, USA;) supplemented with 50 µl/ml Protease Inhibitor Cocktail and 1 mM Phenylmethanesulfonyl fluoride (PMSF; Sigma).

Upon centrifugation at 13.000 g for 10 min at 4°C, the supernatants were collected and the total protein content was quantified by Bio-Rad protein assay (Bio-Rad Laboratories S.r.l., Milan, Italy) following the manufacturer's instructions. Forty micrograms of total proteins were electrophoresed on NuPAGE® 4-12% Bis-Tris Gel (Invitrogen Life Technologies, 200V, 40 min) and blotted onto polyvinylidene difluoride (PVDF) membranes (Invitrogen Life Technologies; 30V, 1 h). The membranes were blocked with Blocking Solution included in the Western Breeze®Chromogenic Western Blot Immunodetection Kit (Invitrogen Life Technologies) for 30 min at RT on rotary shaker and incubated overnight at 4°C with mouse monoclonal anti-α-sma antibody (1:1000; Abcam), rabbit polyclonal anti-Smad3 (1:1000; Cell Signaling Technology, Danvers, MA, USA) rabbit polyclonal anti-TRPC1 (1:1000; Santa Cruz Biotechnology) rabbit polyclonal anti-α-tubulin (1:1000; Cell Signaling Technology) and mouse monoclonal anti-β-actin (1:10000; Sigma) antibodies, assuming α-tubulin or β-actin as control invariant protein. Immunodetection was performed as described in the Western Breeze®Chromogenic Immunodetection protocol (Invitrogen Life Technologies). Densitometric analysis of the bands was performed using ImageJ software (http://rsbweb.nih.gov/ij) and the values normalized to α-tubulin or β-actin.

Electrophysiological recordings

Whole-cell patch-clamp

Electrophysiological analyses were conducted by the whole-cell patch-clamp technique both in current- and voltage-clamp mode. The experiments were performed and recorded with an Axopatch200B amplifier (Axon Instruments,Union City, CA, USA) interfaced to a Digidata 1200 data-acquisition system controlled by Clampex version 6 software (Axon Instruments) as reported previously [17]. In particular fibroblasts adherent to glass coverslips were put in the 35 mm recording chamber and superfused at 20-22 °C at a rate of 1.8 ml/min by a Pump 33 (Harvard Apparatus) with the following physiological bath solution: 140 mM NaCl, 5.4 mM KCl, 1.5 mM $CaCl_2$, 1.2 mM $MgCl_2$, 5.5 mM glucose and 5 mM HEPES/NaOH (pH 7.35). Different channel blockers were used to test the presence of specific ion currents: to record inwardly rectifier K^+ currents (I_{Kir}), 4 mM Cs^+ was applied to the bath solution and 0.5 mM $BaCl_2$ was used to block its occurrence. Stretch Activated Current (I_{SAC}) was blocked by $GdCl_3$ (50 μM; Sigma). The patch pipettes was filled with the following solution: 130 mM KCl, 10 mM NaH_2PO_4, 0.2 mM $CaCl_2$, 1 mM EGTA, 5 mM MgATP and 10 mM HEPES. For bath and pipette solution, pH was set to 7.4 with NaOH and to 7.2 with KOH, respectively. The resistance of the filled pipettes was approximately 6-8 MΩ.

The resting membrane potential (RMP) was recorded by switching to the current clamp mode of the 200B amplifier. In order to record its precise value, we first estimated the junction potential of the electrode prior membrane patch formation; this juction potential value was then subtracted from the recorded membrane potential. The cell linear capacitance (C_m) was evaluated as previously described [17]. C_m value was considered as an index of the cell surface area, assuming that membrane-specific capacitance is constant at 1 μF/cm^2. The current amplitude (I) was normalized to C_m to appropriately compare the test currents recorded in cells of different size; accordingly, I/C_m value is proposed as current density (pA/pF). Linear leak and capacitance currents were cancelled on-line by the P/4 procedure.

Pulse protocols of stimulation

The ionic currents were recorded in voltage clamp mode. The currents flowing through the voltage independent stretch activated channels (I_{SAC}) were estimated by a mathematical procedure. We first evoked the total membrane current $I_{m,}$ by a voltage ramp pulse protocol ranging from -120 to +40 mV at a rate of 100 mV/second, applied from a holding potential (HP) of -40 mV. At the end of any experimental session a commonly used pharmacological Stretch Activated Channel (SAC)

blocker $GdCl_3$ (50 μM; Sigma) was added to the bath solution and the pulse protocol was applied again to record the leak current ($I_{m,leak}$). The Gd^{3+}- sensitive I_{SAC} was thus determined by the point-by-point subtraction of $I_{m,leak}$ from the total current $I_{m,}$ recorded at the beginning of the experiment. This isolated the not voltage-dependent I_{SAC} currents, that were normalized for C_m, to allow the comparison of size different cells. Similarly, we used ramp pulses from -120 to +50 mV (HP = 0 mV), at a rate of 100 mV/sec to evoke I_{Kir}, as previously published [17]. The experiments were repeated in the presence of the blocker Ba^{2+} in the recording solution and the resulting current trace was then subtracted from the one obtained in the absence of Ba^{2+}. The resulting I_{Kir} was then normalized for C_m.

Statistical analysis

Mathematical and statistical analyses of electrophysiological data were performed by pClamp9 (Axon Instruments). For the other data, calculations were performed using GraphPad Prism software (GraphPad, San Diego, CA, USA). Data are expressed as mean ± SEM. Statistical significance was determined by one-way ANOVA and Newman-Keuls multiple comparison test; results were considered statistically significant if $p < 0.05$.

RESULTS

Diode laser irradiation inhibited TGF-β1-induced fibroblast-myofibroblast transition

We evaluated the effects of a low level irradiation with a diode laser at a wavelenght of 635±5 nm on fibroblast-myofibroblast transition. To this aim, NIH/3T3 fibroblasts were cultured in a low serum medium (FBS 2%) for different times (24 h, 48 h or 72 h) in the presence of 2 ng/ml TGF-β1, the well known pro-fibrotic agent [47], in order to promote cell differentiation towards myofibroblasts, irradiated or not with the diode laser using the parameters as reported in Table 1. Cells cultured in the medium supplemented with FBS 10%, not treated with TGF-β1 and not irradiated were used as controls. We found that diode laser did not affect cell viability as judged by MTS assay performed after 24 h from treatment (Fig. 1A). Simultaneously, diode laser irradiation was able to induce a significant increase in proliferation of TGF-β1 treated fibroblasts counteracting the anti-proliferative action of the pro-fibrotic factor, as showed by the increase in the number of the cells positive for Ki67, a nuclear protein marker for cell proliferation (Fig. 1B).

To evaluate the differentiation of fibroblasts into myofibroblasts in our experimental model, we searched for well known myofibroblastic markers such as the presence of stress fibers and the

expression of α-sma and type-1 collagen. The morphological analysis showed that the cells treated with TGF-β1 already after 24 h, exhibited a more organized cytoskeleton as compared to that of control cells, consisting in the presence of robust stress fibres associated with a significant increase in the expression of α-sma, mainly localized along their course (Fig. 2A). As shown by Western blotting analysis and as expected, TGF-β1 induced a further increase in α-sma expression levels after 48 h and 72 h of treatment (Fig. 2B). Moreover the cells exposed for 72 h to TGF-β1 presented an increase in the expression of type-1 collagen at the cytoplasmic level (Fig. 2A) further confirming the capability of TGF-β1 to induce fibroblast-myofibroblast transition. Of note, diode laser irradiation was able to inhibit TGF-β1-induced effect, by reducing the assembly of stress fibers and down-regulating both α-sma and type-1 collagen expression (Fig. 2).

To further support these data, in parallel experiments we evaluated the electrophysiological properties of the cells by whole-cell patch-clamp technique. We first recorded in current clamp mode the resting membrane potential (RMP), a key physiological parameter whose small modifications can substantially change cell excitability, contractility and other properties such as cell migration [17]. RMP of fibroblasts cultured for different times in the presence of TGF-β1, showed that such condition induced a depolarization of RMP with respect to controls (Fig. 3A). By contrast, diode laser stimulation was able to prevent the TGF-β1-induced effect at any time point, evoking a statistically significant hyperpolarization of RMP whose values returned to the ones recorded in controls (Fig. 3A). We then analyzed in voltage clamp mode the cell capacitance (C_m), usually assumed as index of cell surface. C_m increased with respect to control cells in both TGF-β1 treated cells and TGF-β1 and diode laser treated ones at any time, consistent with an increase of the individual cell size during myofibroblast differentiation (Fig. 3B). However, diode laser stimulation was not able to induce any significant change of C_m values respect to TGF-β1 treatment alone. According to our previously work [17] we also tested the effects of the cell treatments on the inward rectifying K^+ current, I_{Kir}, usually well expressed in myofibroblasts. We observed that in response to voltage ramp pulse stimulation (as described in Methods), the cells treated with TGF-β1 showed a consistent Ba^{2+} -sensitive I_{kir} for negative voltages, and that the amplitude of this current was significantly reduced after diode laser stimulation (Fig. 4).

Diode laser stimulation modulated the expression of MMPs and of TIMPs in TGF-β1-treated fibroblasts

A fine coordination between a family of proteolytic enzymes that selectively digest individual components of ECM, namely MMPs, and their specific tissue inhibitors (TIMPs) is crucial for

connective tissue remodelling after a tissue damage and for counteracting the excessive deposition of collagen by myofibroblasts [11]. On this basis, we investigated whether diode laser stimulation could modulate the expression and activity of MMP-2 /MMP-9 and TIMP-1/TIMP-2 in fibroblasts. As determined by confocal immunofluorescence analyses, we found that control NIH/3T3 cells expressed all these enzymes: in particular MMP-9 was concentrated along cytoskeletal filaments, MMP-2 was mainly distributed inside the cytoplasm as well as TIMP-1 and TIMP-2 (Fig. 5). The cells treated with TGF-β1 for 24 h displayed a reduction of the expression of both MMP-2 and MMP-9 associated with an increase of TIMP-1 and TIMP-2 as compared to control cells (Fig. 5). Of note, diode laser irradiation was able to revert TGF-β1 induced effect, by up-regulating MMP-2 and MMP-9 expression and down-regulating TIMP-1 and TIMP-2 (Fig. 5).

Diode laser–induced prevention of fibroblast-myofibroblast transition is mediated by the Transient Receptor Potential Canonical Channel 1 (TRPC1) functionality

It has been recently reported that TGF-β1 affects the functionality of different ion channels including Transient Receptor Potential (TRP) channels and that TRP-mediated calcium influx is required to promote fibroblast–myofibroblast transition [48,49].

Based on these data, in order to investigate the mechanisms by which diode laser irradiation could influence fibroblast differentiation, we analyzed the expression and activity of TRPC1 in our experimental conditions. TRPC1 belongs to the superfamyly of TRP protein, acting as Store-Operated Ca^{2+} entry Channel (SOC) in various cell types [50], and also as Stretch Activated Channel (SAC) [46].

Confocal immunofluorescence analysis showed a positive labeling of TRPC1 in the cytoplasm and plasmamembrane of control NIH/3T3 fibroblasts and a significant increase of the immunstaining in the cells treated with TGF-β1 (Fig. 6A). In particular TRPC1 expression gradually increased with time reaching maximal levels after 48-72 h of treatment. The parallel electrophysiological recordings were in agreement with the morphological analyses; in fact TGF-β1 treated fibroblasts regularly showed linear currents ascribable to non selective cation currents or TRPC1 fluxes through SACs (I_{SAC}) according to our previously reported data [46] (Fig. 6B).

These results suggested a role for TRPC1 channels in the fibroblast-myofibroblast transition. To support these data we then analyzed the expression of α-sma in cells in which TRPC1 gene expression was silenced with a specific TRPC1-siRNA, or the channel activity was pharmacologically blocked with 50 μM $GdCl_3$. As judged by confocal immunofluorescence and Western blotting analyses the expression of the myofibroblast marker appeared significantly reduced when either the gene expression of TRPC1 was down-regulated or its activity blocked (Fig.

7). It was worth noting that diode laser irradiation was able to reduce the increase of TRPC1 expression and activity in TGF-β1 treated cells at any time (Fig. 6) and to induce a further decrease of α-sma expression in the cells silenced for TRPC1 or treated with $GdCl_3$ as compared to the laser unstimulated ones (Fig. 7). All these data suggested that diode laser-induced inhibition of fibroblast-myofibroblast transition could be, at least in part, mediated by the TRPC1 functionality. Finally, we also demonstrated that diode laser irradiation and TRPC1 expression and activity could exert their inhibitory effects on fibroblast differentiation by interfering with TGF-β1 mediated intracellular signaling pathway, since the diode laser treatment (Fig. 8A) as well as the inhibition of TRPC1 (Fig. 8B) caused a significant decrease in the expressionof Smad3, the TGF-β1 downstream signaling molecule, in TGF-β1-treated cells.

DISCUSSION

The beneficial effect of LLLT or photobiomodulation therapy in ameliorating fibrosis has been recently demonstrated in different damaged and diseased organs including kidney, skeletal muscle, skin, heart and tendon, but little is known concerning the cellular and molecular mechanisms by which the laser could exert this action [27,28,33,39-45].

Most of the studies in this field suggest that the cellular responses to laser therapy are mediated by the classical mechanisms mainly involving changes in the activity of mitochondria. In fact, mitochondria contain cytochromes and porphyrins of the respiratory chain which act as light receptors and are therefore believed to be the primary phototargets during irradiation. In particular, photon absorption results in the modulation of reactive oxygen species (ROS) production and in an increase of ATP synthesis leading to regulation of the cell function, cytoprotection and, in turn, attenuation of inflammation and fibrosis [26,39,40,45,51].

Data of the present study, beside supporting the anti-fibrotic effect of the photobiomodulation, contribute to add new insights into the cellular and molecular targets of the laser. Indeed, we have provided experimental evidence for the ability of photobiomodulation therapy with a 635±5 nm diode laser, to inhibit TGF-β1 induced fibroblast-myofibroblast transition *in vitro* by modulating the expression and the activity of TRPC1 membrane channel and interfering with TGF-β1 signaling.

It is well established that myofibroblasts are the major contributors to tissue scarring [12]. These cells combine immunophenotypical and ultrastructural features of fibroblasts and smooth muscle cells by exhibiting *de novo* formation and deployment of contractile actin/myosin- containing stress fibers and expression of α-sma with the extensive endoplasmic reticulum of synthetically–active fibroblasts. They respond to different stimuli including mechanical stress, hypoxia, paracrine factors

by increasing synthesis and deposition of ECM proteins and exerting traction forces on ECM [2,12]. Fibroblast-myofibroblast transition is a key mechanism in the normal reparative response to tissue damage and the myofibroblast activity is beneficial for restoring the tissue integrity through the formation of a contractile scar. For example, scars stabilize the heart muscle after myocardial infarction as well as tendon, bone, and cartilage after fracture or rupture. However, persistence of myofibroblasts in the wound as well as deregulated and chronic activity of these cells, leads to fibrosis and organ failure [12]. Given that myofibroblast generation is a crucial event shared by fibrosis in all organs, its inhibition could represent an effective non-organ-specific tool, to counteract fibrosis.

In such a view, our data, demonstrating that the diode laser induced inhibition of fibroblast-myofibroblast transition, appear intriguing and of potential clinical interest. In particular, our results have shown that diode laser stimulation of TGF-β1-treated NIH/3T3 fibroblasts, affects multiple processes associated with fibroblast differentiation, namely *i)* inhibition of the assembly of stress fibers; by these structures the myofibroblast is capable to remodel and contract the ECM and also to adapt its activity to changes in the mechanical microenvironment as occur in fibrotic tissue [12,52]; *ii)* reduction of α-sma and type-1 collagen expression; *iii)* modification of plasmamembrane passive properties and ion currents typically expressed by myofibroblasts. In particular, laser stimulation counteracted the tendency of TGF-β1 to induce a depolarization of RPM, strictly correlated with the proliferation and contractile properties of myofibroblasts [53], causing an hyperpolarization of this parameter, and attenuated inwardly rectifying K^+ currents (I_{Kir}), which usually increase in the transition to myofibroblasts and are determinant of RMP and thus of myofibroblast contractility [17,53].

It is well known that a fine coordination between MMPs and TIMPs is also essential to counteract the excessive deposition of collagen by myofibroblasts and maintain the homeostasis of ECM [11] Therefore our data, showing the capability of the laser to up-regulate the expression of MMP-2 and MMP-9 while concomitantly down-regulating the expression of their specific tissue inhibitors TIMP-1 and TIMP-2, add further evidence to the ability of photobiomodulation therapy to affect ECM remodeling. This is in accordance with previous finding on the positive effect of LLLT on MMP-2 gelatinolytic activity during the skeletal muscle regeneration process [44,54].

Although many cytokines and growth factors can stimulate fibroblast-myofibroblast transition, TGF-β1 is the most effective pro-fibrotic cytokine secreted by various cell types in the lesion site, including epithelial cells, platelets, macrophages, fibroblasts and also myofibroblasts. Indeed, autocrine TGF-β1 secretion by myofibroblasts sustains a vicious cycle, which further promotes their differentiation and the progression of fibrosis [13,47,55]. Moreover, there is

evidence supporting the concept that myofibroblasts could promote fibrogenic signaling also via a contractile force-mediated activation of latent TGF-β1 bound to the ECM. In this process, contractility generated by stress fibers is transmitted from the cytoskeleton to the ECM through the transmembrane integrins and this force transmission causes a conformational change of the ECM-bound latent TGF-β1 complex, thus leading to the release (or exposure) of active TGF-β1 which is then able to bind to its receptor(s) [56].

TGF-β1 promotes fibroblast-myofibroblast differentiation and myofibroblast survival by inducing a variety of signaling pathways, including the canonical TGF-β1 signaling pathway (Smad2/3-dependent) and non-canonical pathways, such as PI3K/AKT/mTOR pathway [47]. Our data, showing a reduction of Smad3 expression in the fibroblast irradiated with the diode laser, suggest that laser could exert its inhibitory effects on myofibroblast generation by interfering with the canonical TGF-β1 mediated intracellular signaling pathway. These data are in agreement with previuos studies demonstrating the contribution of photobiomodulation therapy in preventing fibrosis by decreasing TGF-β1 mRNA expression [57,58] in an injured skeletal muscle and of Smad3 expression in an animal model of renal interstitial fibrosis [41].

Moreover this study adds new insights into the molecular targets of the laser suggesting, for the first time, that diode laser could promote the inhibition of TGF-β1 induced myofibroblast generation by modulating TRPC1 ion channel functionality. In particular, we observed that the expression and the activity of TRPC1 ion channel significantly augmented in TGF-β1-treated fibroblasts and that the pharmacological block of this channel as well as the silencing of TRPC1 gene expression reduced myofibroblast differentiation. Notably, the diode laser irradiation was able to prevent the increase of TRPC1 ion channel expression and activity induced by TGF-β1. In line with this, previous data have shown the ability of LLLT to modulate TRP channel functionality in other cell types; in particular it has been demonstrated a modulation of TRPC1 functionality by a low pulse energy Nd:YAG laser irradiation in osteoblastic cells [24] and of Transient Receptor Potential Vanilloid 4 (TRPV4) channels by a 405 nm laser in mast cell line [59]. Our data are also consistent with the studies in the literature demonstrating that TGF-β1 regulates different TRP channels including TRPC1 in fibroblasts from different organs [48,60,61] and that TRPC-mediated calcium signaling plays an important role in the differentiation of fibroblasts to myofibroblasts and in fibrogenesis cascade [48,49,62-64].

Moreover, given that differentiation of fibroblastic cells towards the myofibroblastic phenotype is also dependent on mechanical stimuli derived from ECM [12] and that TRPC1 has been demonstrated to be a component of Stretch Activated Channels (SACs) acting as mechanotrasductor [46], it is worth to suggest that this channel could be involved in the myofibroblast generation for

its ability to integrate signals from TGF-β1 and mechanical factors as reported for other classes of TRP channels [65].

How laser irradiation could affect TRPC1 functionality still remains to be elucidated. Since TRP proteins were first found in the eye of a Drosophila mutant and are required for maintaining the light response [66], it can be hypothesized that TRPC1 can directly absorb photons to regulate its activity, but to our knowledge there are no studies in the literature on the effects of the light stimulation on isolated mammalian TRPC proteins. On the other hand, it can be supposed that the laser-induced inhibition of TRPC1 expression and activity could be correlated to the reported ability of the laser to prevent oxidative stress reducing the generation of reactive oxygen species (ROS) [27,40] whose levels have been demonstrated to be regulated by TGF-β1 [4,67] and involved in TRPC1 activation [68,69]. Moreover, it can be also speculated that the mechanisms underlying the laser-mediated channel functionality in fibroblast cells, may involve alterations of mechanical properties of the cell surface followed by TRPC1 channel down-regulation, intracellular calcium changes and inhibition of TGF-β1/Smad3 signaling pathway. Further studies are required to define the real mechanism of TRPC1 activation by laser irradiation.

In conclusion, the results of this study provide novel insights into the cellular and molecular mechanisms by which a LLLT with a 635±5 nm diode laser could exert an anti-fibrotic action and may contribute to add information on the potentials of this therapy, as a new treatment option for tissue fibrosis.

FIGURE LEGEND

Fig. 1. Effect of diode laser irradiation on viability and proliferation of TGF-β1 treated NIH/3T3 fibroblasts. The cells were cultured for 24 h in low serum (FBS 2%) in the presence of 2 ng/ml TGF-β1, irradiated or not with diode laser for 10 s or 26 s as reported in Table 1. Control cells were cultured in growth medium (FBS 10%). A) MTS cell viability assay. Otpical density of soluble colored formazan produced by MTS reduction, was evaluated using a multi-well scanning spectrophotometer at 492 nm. B) Evaluation of cell proliferation by confocal immunofluorescence analysis of Ki67 expression. The histogram shows the number of the cells with Ki67 positive nuclei expressed as percentage of the total nuclei number. Data shown are mean ± SEM and represent the results of at five independent experiments performed in triplicate. Significance of difference evaluated by one-way ANOVA and Newman–Keuls multiple comparison test: * $p< 0.05$ vs CONTROL (FBS 10%); ° $p < 0.05$ *vs* FBS 2% + TGF-β1.

Fig. 2. Effect of diode laser irradiation on fibroblast-myofibroblast transition. NIH/3T3 fibroblasts were cultured for 24 h, 48 h and 72 h in low serum (FBS 2%) in the presence of 2 ng/ml TGF-β1, irradiated or not with diode laser for 26 s as reported in Table 1 (*treated surface diameter: 30 mm*). Control cells were cultured in growth medium (FBS 10%). A) Representative confocal fluorescence images of the cells in the indicated experimental conditions, stained with TRITC-conjugated phalloidin to reveal F-actin (red) or immunostained with antibodies against α-sma (green) or type-1 collagen (cyan). Nuclei are counterstained in red with propidium iodide (PI). The histograms show the densitometric analyses of the intensity of the fluorescence signals for each specific marker performed on digitized images. Scale bar = 25 µm. B) Western blotting analysis of α-sma expression in fibroblasts in the indicated experimental conditions. The densitometric analysis of the bands normalized to α-tubulin is reported in the histogram. Data shown are mean ± SEM and represent the results of at least three independent experiments performed in triplicate. Significance of difference evaluated by one-way ANOVA and Newman–Keuls multiple comparison test: * $p< 0.05$ *vs* CONTROL (FBS 10%); ° $p <0.05$ *vs* FBS 2% + TGF-β1; # $p <0.05$ *vs* previous time.

Fig. 3. Effect of diode laser irradiation on electrophysiological plasmamembrane properties of TGF-β1 treated NIH/3T3 fibroblasts. NIH/3T3 fibroblasts were cultured for 24 h, 48 h and 72 h in low serum (FBS 2%) in the presence of 2 ng/ml TGF-β1, irradiated or not with diode laser for 26 s as reported in Table 1 (*treated surface diameter: 30 mm*). Control cells were cultured in growth medium (FBS 10%). A) Resting membrane potential (RMP) recorded by whole-cell patch-clamp technique in current clamp mode. B) Cell capacitance (C_m) commonly used as index of cell size, recorded by whole-cell patch-clamp technique in voltage clamp mode. Data are the mean ± SEM: CONTROL (FBS 10%), n = 20 cells; FBS 2% + TGF-β1, n = 30 cells; FBS 2% + TGF-β1 + LASER, n = 30 cells. Significance of difference evaluated by one-way ANOVA and Newman–Keuls multiple comparison test :* $p< 0.05$ *vs* CONTROL (FBS 10%); ° $p <0.05$ *vs* FBS 2% + TGF-β1 treatment at the same time.

Fig. 4. Effect of diode laser irradiation on delayed rectifier total outward K^+ currents ($I_{K,DR}$) on TGF-β1 treated NIH/3T3 fibroblasts.

I-V plot related to the inward rectifying K^+ currents (I_{Kir}), obtained in response to ramp voltage pulse stimulation (HP = 0 mV) applied to fibroblasts cultured for 72 h in low serum (FBS 2%) in the presence of 2 ng/ml TGF-β1 (blue trace) and to TGF-β1 treated fibroblasts irradiated with the diode laser (red trace) for 26 s as reported in Table 1 (*treated surface diameter: 30 mm*). Each trace was obtained by pharmacological dissection in the presence of Kir channel blocker (Barium Chloride), subtracting the current recorded in the bath recording solution from that recorded in control solution. Current amplitude values were normalized for cell capacitance (C_m). Data are expressed as mean ± SEM (FBS 2% + TGF-β1, n = 22 cells; FBS 2% + TGF-β1 + LASER, n = 22 cells). Significance of difference evaluated by one-way ANOVA and Newman–Keuls multiple comparison test: * $p <0.05$ *vs* FBS 2% + TGF-β1 + LASER.

Fig. 5. Effect of diode laser irradiation on MMP-2, MMP-9, TIMP-1 and TIMP-2 expression in TGF-β1 treated NIH/3T3 fibroblasts. Representative immunofluorescence confocal images of NIH/3T3 fibroblasts cultured in growth medium (CONTROL, FBS 10%) or cultured for 24 h in low

serum medium (FBS 2%) in the presence of 2 ng/ml TGF-β1, irradiated or not with diode laser for 26 s as reported in Table 1 (*treated surface diameter: 30 mm*) and immunostained with antibodies against MMP-9 (red), MMP-2 (green), TIMP-1 (cyan) and TIMP-2 (green). Scale bar = 25 µm. Densitometric analyses of the intensity of the specific fluorescence signals performed on digitized images are reported in the histograms. Data shown are mean ± SEM and represent the results of at least three independent experiments performed in duplicate. Significance of difference evaluated by one-way ANOVA and Newman–Keuls multiple comparison test: * $p< 0.05$ *vs* CONTROL (FBS 10%); ° $p < 0.05$ *vs* FBS 2% + TGF-β1.

Fig. 6. Effect of diode laser irradiation on TRPC1 expression and on currents through TRPC1 (I_{SAC}) in TGF-β1 treated NIH/3T3 fibroblasts. NIH/3T3 fibroblasts were cultured for 24 h, 48 h and 72 h in low serum (FBS 2%) in the presence of 2 ng/ml TGF-β1, irradiated or not with diode laser for 26 s as reported in Table 1 (*treated surface diameter: 30 mm*). Control cells were cultured in growth medium (FBS 10%). A) Representative confocal fluorescence images of the cells in the indicated experimental conditions stained with TRITC-conjugated phalloidin to reveal F-actin (red) and immunostained with antibodies against TRPC1 (green). Scale bar = 50 µm. The histogram shows the densitometric analyses of the intensity of the TRPC1 fluorescence signal performed on digitized images. Data shown are mean ± SEM and represent the results of at least three independent experiments performed in triplicate. B) I-V plot related to the non selective cation currents fluxes through SACs (I_{SAC}), obtained in response to ramp voltage pulse stimulation (HP = -40 mV) applied to fibroblasts cultured for 72 h in low serum (FBS 2%) in the presence of 2 ng/ml TGF-β1 not irradiated (green trace) or irradiated with diode laser (violet trace). Current amplitude is normalized for cell capacitance (C_m). Data are mean ± SEM (FBS 2% + TGF-β1, n = 20 cells; FBS 2% + TGF-β1 + LASER, n = 20 cells). Significance of difference evaluated by one-way ANOVA and Newman–Keuls multiple comparison test. In A: * $p< 0.05$ *vs* CONTROL (FBS 10%); ° $p < 0.05$ *vs* FBS 2% + TGF-β1; # $p < 0.05$ *vs* previous time. In B * $p < 0.05$ vs FBS 2% + TGF-β1 + LASER.

Fig. 7. Effect of inhibition of TRPC1 expression and functionality on fibroblast-myofibroblast transition. To inhibit TRPC1 gene expression NIH/3T3 fibroblasts were silenced by specific TRPC1-siRNA cultured for 24 h in low serum (FBS 2%) in the presence of 2 ng/ml TGF-β1, irradiated or not with diode laser for 26 s as reported in Table 1 (*treated surface diameter: 30 mm*), SCR-siRNA was used as control. In other experiments the cells in low serum medium were pre-treated with Gadolinium Chloride (50 μM, $GdCl_3$) a specific SAC channel blocker, before TGF-β1 addition and irradiation or not with diode laser. A) Representative confocal immuofluorescence images of the cells in the indicated experimental conditions immunostained with antibodies against TRPC1 (red, upper panel) and α-sma (green). Propidium iodide (PI, red) was used to counterstain nuclei. Scale bar = 50 μm. The histograms show the densitometric analyses of the intensity of the fluorescence signal for specific markers performed on digitized images. B) Western blotting analysis of α-sma expression in fibroblasts in the indicated experimental conditions. The densitometric analysis of the bands normalized to α-tubulin is reported in the histograms. Data shown are mean ± SEM and represent the results of at least three independent experiments performed in triplicate. Significance of difference evaluated by one-way ANOVA and Newman–Keuls multiple comparison test: * $p< 0.05$ *vs* SCR-siRNA + TGF-β1; ° $p < 0.05$ *vs* SCR-siRNA + TGF-β1 + LASER; # $p < 0.05$ *vs* FBS 2% + TGF-β1; § $p < 0.05$ *vs* $GdCl_3$ + TGF-β1; & $p < 0.05$ *vs* FBS 2% + TGF-β1 + LASER.

Fig. 8. Effect of inhibition of TRPC1/SAC expression and functionality on TGF-β1/Smad3 signaling pathway. Western blotting analysis of Smad3 expression in NIH/3T3 fibroblasts A) cultured for 24 h, 48 h and 72 h in low serum (FBS 2%) in the presence of 2 ng/ml TGF-β1, irradiated or not with diode laser for 26 sec as reported in Table 1 *(treated surface diameter: 30 mm)* or in growth medium (CONTROL, FBS 10%); B) -*left panel*- cultured in low serum medium for 24 h, pre-treated with Gadolinium Chloride (50 μM, $GdCl_3$) a specific SAC channel blocker, before TGF-β1 addition and irradiated or not with diode laser and -*right panel*- silenced for TRPC1 by specific TRPC1-siRNA and cultured for 24 h in low serum in the presence of TGF-β1 irradiated or not with diode laser. SCR-siRNa was used as control. The densitometric analyses of the bands

normalized to β-actin are reported in the histograms. Data shown are mean ± SEM and represent the results of at least three independent experiments performed in triplicate. Significance of difference evaluated by one-way ANOVA and Newman–Keuls multiple comparison test: * $p< 0.05$ *vs* CONTROL (FBS 10%), ° $p < 0.05$ *vs* FBS2% + TGF-β1; # $p < 0.05$ *vs* previous time; § $p < 0.05$ *vs* $GdCl_3$ + TGF-β1; % $p < 0.05$ *vs* SCR-siRNA + TGF-β1; $ $p < 0.05$ *vs* TRPC1-siRNA + TGF-β1.

REFERENCES

1. Zeisberg M, Kalluri R. Cellular Mechanisms of Tissue Fibrosis. 1. Common and organ-specific mechanisms associated with tissue fibrosis. Am J Physiol Cell Physiol 2013;304(3):C216–C225.
2. Borthwick LA, Wynn TA, Fisher AJ. Cytokine mediated tissue fibrosis. Biochim Biophys Acta 2013;1832(7):1049-1060.
3. Serrano AL, Muñoz-Cánoves P. Regulation and dysregulation of fibrosis in skeletal muscle. Exp Cell Res 2010;316:3050–3058.
4. Barnes JL, Gorin Y. Myofibroblast differentiation during fibrosis: role of NAD(P)H oxidases. Kidney Int 2011;79(9):944-956.
5. Mallat A, Lotersztajn S. Cellular mechanisms of tissue fibrosis. 5. Novel insights into liver fibrosis. Am J Physiol Cell Physiol 2013;305(8):C789-C799.
6. Helling BA, Yang IV. Epigenetics in lung fibrosis: from pathobiology to treatment perspective. Curr Opin Pulm Med 2015;21(5):454-462.
7. López B, González A, Ravassa S, Beaumont J, Moreno MU, San José G, Querejeta R, Díez J. Circulating Biomarkers of Myocardial Fibrosis: The Need for a Reappraisal. J Am Coll Cardiol 2015;65(22):2449-2456.
8. Rinkevich Y, Walmsley GG, Hu MS, Maan ZN, Newman AM, Drukker M, Januszyk M, Krampitz GW, Gurtner GC, Lorenz HP, Weissman IL, Longaker MT. Skin fibrosis. Identification and isolation of a dermal lineage with intrinsic fibrogenic potential. Science 2015; 348(6232):aaa2151.
9. Otranto M1, Sarrazy V, Bonté F, Hinz B, Gabbiani G, Desmoulière A. The role of the myofibroblast in tumor stroma remodeling. Cell Adh Migr 2012;6(3):203-219.
10. Wollina U, Verma SB, Ali FM, Patil K.Oral submucous fibrosis: an update. Clin Cosmet Investig Dermatol 2015;8:193-204.
11. Arpino V, Brock M, Gill SE. The role of TIMPs in regulation of extracellular matrix proteolysis. Matrix Biol 2015;44-46C:247-254.
12. Hinz B. Myofibroblasts. Exp Eye Res 2015; [Epub ahead of print].
13. Rosenbloom J, Mendoza FA, Jimenez SA. Strategies for anti-fibrotic therapies. Biochim Biophys Acta 2013;1832(7):1088-1103.
14. Tsou PS, Haak AJ, Khanna D, Neubig RR. Cellular mechanisms of tissue fibrosis. 8. Current and future drug targets in fibrosis: focus on Rho GTPase-regulated gene transcription. Am J Physiol Cell Physiol 2014;307(1):C2-C13.
15. Spagnolo P, Maher TM, Richeldi L. Idiopathic pulmonary fibrosis: Recent advances on pharmacological therapy. Pharmacol Ther 2015;152:18-27.
16. Sassoli C, Chellini F, Pini A, Tani A, Nistri S, Nosi D, Zecchi-Orlandini S, Bani D, Formigli L. Relaxin prevents cardiac fibroblast-myofibroblast transition via notch-1-mediated

inhibition of TGF-β/Smad3 signaling. PLoS One 2013;8(5):e63896.

17. Squecco R, Sassoli C, Garella R, Chellini F, Idrizaj E, Nistri S, Formigli L, Bani D, Francini F. Inhibitory effects of relaxin on cardiac fibroblast-to-myofibroblast transition: an electrophysiological study. Exp Physiol 2015;100(6):652-666.
18. Frati A, Ricci B, Pierucci F, Nistri S, Bani D, Meacci E. Role of sphingosine kinase/S1P axis in ECM remodeling of cardiac cells elicited by relaxin. Mol Endocrinol 2015;29(1):53-67.
19. Huuskes BM, Wise AF, Cox AJ, Lim EX, Payne NL, Kelly DJ, Samuel CS, Ricardo SD. Combination therapy of mesenchymal stem cells and serelaxin effectively attenuates renal fibrosis in obstructive nephropathy. FASEB J 2015;29(2):540-553.
20. Sassoli C, Zecchi-Orlandini S, Formigli L. Trophic actions of bone marrow-derived mesenchymal stromal cells for muscle repair/regeneration. Cells 2012;1(4):832-850.
21. Fedak PW, Bai L, Turnbull J, Ngu J, Narine K, Duff HJ. Cell therapy limits myofibroblast differentiation and structural cardiac remodeling: basic fibroblast growth factor-mediated paracrine mechanism. Circ Heart Fail 2012;5:349-356.
22. Sassoli C, Nosi D, Tani A, Chellini F, Mazzanti B, Quercioli F, Zecchi-Orlandini S, Formigli L. Defining the role of mesenchymal stromal cells on the regulation of matrix metalloproteinases in skeletal muscle cells. Exp Cell Res 2014;323(2):297-313.
23. Giannelli M, Bani D, Tani A, Pini A, Margheri M, Zecchi-Orlandini S, Tonelli P, Formigli L. In vitro evaluation of the effects of low-intensity Nd:YAG laser irradiation on the inflammatory reaction elicited by bacterial lipopolysaccharide adherent to titanium dental implants. J Periodontol 2009;80(6):977-984.
24. Chellini F, Sassoli C, Nosi D, Deledda C, Tonelli P, Zecchi-Orlandini S, Formigli L, Giannelli M. Low pulse energy Nd:YAG laser irradiation exerts a biostimulative effect on different cells of the oral microenvironment: "an in vitro study". Lasers Surg Med 2010;42(6):527-539.
25. Giannelli M, Chellini F, Sassoli C, Francini F, Pini A, Squecco R, Nosi D, Bani D, Zecchi-Orlandini S, Formigli L. Photoactivation of bone marrow mesenchymal stromal cells with diode laser: effects and mechanisms of action. J Cell Physiol 2013;228(1):172-181.
26. Basso FG, Oliveira CF, Kurachi C, Hebling J, Costa CA. Biostimulatory effect of low-level laser therapy on keratinocytes in vitro. Lasers Med Sci 2013;28(2):367-374.
27. Avci P, Gupta A, Sadasivam M, Vecchio D, Pam Z, Pam N, Hamblin MR. Semin Cutan Med Surg. Low-level laser (light) therapy (LLLT) in skin: stimulating, healing, restoring Semin Cutan Med Surg 2013;32(1):41-52.
28. Jin R, Huang X, Li H, Yuan Y, Li B, Cheng C, Li Q. Laser therapy for prevention and treatment of pathologic excessive scars. Plast Reconstr Surg 2013;132(6):1747-1758.
29. Pandeshwar P, Roa MD, Das R, Shastry SP, Kaul R, Srinivasreddy MB.

Photobiomodulation in oral medicine: a review. J Investig Clin Dent 2015; [Epub ahead of print].

30. Barbosa RI, Marcolino AM, de Jesus Guirro RR, Mazzer N, Barbieri CH, de Cássia Registro Fonseca M. Comparative effects of wavelengths of low-power laser in regeneration of sciatic nerve in rats following crushing lesion. Lasers Med Sci 2010;25:423-430.
31. Oron U, Maltz L, Tuby H, Sorin V, Czerniak A. Enhanced liver regeneration following acute hepatectomy by low-level laser therapy. Photomed Laser Surg 2010;28(5):675-678.
32. Fávaro-Pípi E, Ribeiro DA, Ribeiro JU, Bossini P, Oliveira P, Parizotto NA, Tim C, de Araújo HS, Renno AC. Low-level laser therapy induces differential expression of osteogenic genes during bone repair in rats.Photomed Laser Surg 2011;29:311-317.
33. da Rosa AS, dos Santos AF, da Silva MM, Facco GG, Perreira DM, Alves AC, Leal Junior EC, de Carvalho Pde T. Effects of low-level laser therapy at wavelengths of 660 and 808 nm in experimental model of osteoarthritis. Photochem Photobiol 2012;88(1):161-166.
34. Hoffman M, Monroe DM. Low intensity laser therapy speeds wound healing in hemophilia by enhancing platelet procoagulant activity. Wound Repair Regen 2012;20:770-777.
35. Alves AN, Fernandes KP, Deana AM, Bussadori SK, Mesquita-Ferrari RA. Effects of low-level laser therapy on skeletal muscle repair: a systematic review.Am J Phys Med Rehabil 2014;93(12):1073-1085.
36. Amid R, Kadkhodazadeh M, Ahsaie MG, Hakakzadeh A. Effect of low level laser therapy on proliferation and differentiation of the cells contributing in bone regeneration. J Lasers Med Sci 2014;5(4):163-170.
37. de Loura Santana C, de Fátima Teixeira Silva D, Deana AM, Prates RA, Souza AP, Gomes MT, de Azevedo Sampaio BP, Shibuya JF, Bussadori SK, Mesquita-Ferrari RA, Fernandes KP, França CM. Tissue responses to postoperative laser therapy in diabetic rats submitted to excisional wounds. PLoS One 2015;10(4):e0122042.
38. Giannelli M, Bani D, Viti C, Tani A, Lorenzini L, Zecchi-Orlandini S, Formigli L. Comparative evaluation of the effects of different photoablative laser irradiation protocols on the gingiva of periodontopathic patients. Photomed Laser Surg 2012;30(4):222-230.
39. Oron U, Yaakobi T, Oron A, Mordechovitz D, Shofti R, Hayam G, Dror U, Gepstein L, Wolf T, Haudenschild C, Haim SB. Low-energy laser irradiation reduces formation of scar tissue after myocardial infarction in rats and dogs. Circulation 2001;103:296–301.
40. Fillipin LI, Mauriz JL, Vedovelli K, Moreira AJ, Zettler CG, Lech O, Marroni NP, González-Gallego J. Low-level laser therapy (LLLT) prevents oxidative stress and reduces fibrosis in rat traumatized Achilles tendon. Lasers Surg Med 2005;37:293-300.
41. Oliveira FA, Moraes AC, Paiva AP, Schinzel V, Correa-Costa M, Semedo P, Castoldi A, Cenedeze MA, Oliveira RS, Bastos MG, Câmara NO, Sanders-Pinheiro H. Low-level laser therapy decreases renal interstitial fibrosis. Photomed Laser Surg 2012;30(12):705-713.

42. Oliveira Sampaio SC, de C Monteiro JS, Cangussu´ MC, Pires Santos GM, dos Santos MA, dos Santos JN, Pinheiro AL. Effect of laser and LED phototherapies on the healing of cutaneous wound on healthy and iron-deficient Wistar rats and their impact on fibroblastic activity during wound healing. Lasers Med Sci 2013;28:799-806.
43. Leal-Junior EC, de Almeida P, Tomazoni SS, de Carvalho Pde T, Lopes-Martins RÁ, Frigo L, Joensen J, Johnson MI, Bjordal JM. Superpulsed low-level laser therapy protects skeletal muscle of mdx mice against damage, inflammation and morphological changes delaying dystrophy progression. PLoS One 2014;9(3):e89453.
44. Alves AN, Fernandes KP, Melo CA, Yamaguchi RY, França CM, Teixeira DF, Bussadori SK, Nunes FD, Mesquita-Ferrari RA. Modulating effect of low level-laser therapy on fibrosis in the repair process of the tibialis anterior muscle in rats. Lasers Med Sci 2014;29(2):813-821.
45. Mamalis A, Garcha M, Jagdeo J. Light emitting diode-generated blue light modulates fibrosis characteristics: fibroblast proliferation, migration speed, and reactive oxygen species generation. Lasers Surg Med 2015;47(2):210-215.
46. Formigli L, Sassoli C, Squecco R, Bini F, Martinesi M, Chellini F, Luciani G, Sbrana F, Zecchi-Orlandini S, Francini F, Meacci E. Regulation of transient receptor potential canonical channel 1 (TRPC1) by sphingosine 1-phosphate in C2C12 myoblasts and its relevance for a role of mechanotransduction in skeletal muscle differentiation. J Cell Sci 2009;122(Pt 9):1322-1333.
47. Biernacka A, Dobaczewski M, Frangogiannis NG. TGF-β signaling in fibrosis. Growth Factors 2011;29(5):196-202.
48. Ikeda K, Nakajima T, Yamamoto Y, Takano N, Tanaka T, Kikuchi H, Oguri G, Morita T, Nakamura F, Komuro I.Roles of transient receptor potential canonical (TRPC) channels and reverse-mode Na+/Ca2+ exchanger on cell proliferation in human cardiac fibroblasts: effects of transforming growth factor β1. Cell Calcium 2013;54(3):213-225.
49. Yue Z, Zhang Y, Xie J, Jiang J, Yue L. Transient receptor potential (TRP) channels and cardiac fibrosis. Curr Top Med Chem 2013;13(3):270-282.
50. Cheng KT, Ong HL, Liu X, Ambudkar IS. Contribution and regulation of TRPC channels in store-operated Ca2+ entry. Curr Top Membr 2013;71:149-179.
51. Zungu IL, Hawkins Evans D, Abrahamse H.Mitochondrial responses of normal and injured human skin fibroblasts following low level laser irradiation--an in vitro study.Photochem Photobiol 2009;85(4):987-996.
52. Mar PK, Roy P, Yin HL, Cavanagh HD, Jester JV.Stress fiber formation is required for matrix reorganization in a corneal myofibroblast cell line. Exp Eye Res 2001;72(4):455-466.
53. Chilton L, Ohya S, Freed D, George E, Drobic V, Shibukawa Y, MacCannell KA, Imaizumi Y, Clark RB, Dixon IMC, Giles WR. K+ currents regulate the resting membrane potential,

proliferation, and contractile responses in ventricular fibroblasts and myofibroblasts. Am J Physiol Heart Circ Physiol 2005;288:H2931–H2939.

54. Ribeiro BG, Alves AN, Santos LA, Fernandes KP, Cantero TM, Gomes MT, França CM, Silva DF, Bussadori SK2, Mesquita-Ferrari RA. The effect of low-level laser therapy (LLLT) applied prior to muscle injury. Lasers Surg Med 2015; [Epub ahead of print]
55. Uhal BD, Kim JK, Li X, Molina-Molina M. Angiotensin-TGF-beta 1 crosstalk in human idiopathic pulmonary fibrosis: autocrine mechanisms in myofibroblasts and macrophages. Curr Pharm Des 2007;13(12):1247-1256.
56. Wipff PJ, Rifkin DB, Meister JJ, Hinz B. Myofibroblast contraction activates latent TGF-beta1 from the extracellular matrix. J Cell Biol 2007;179(6):1311-1323.
57. Mesquita-Ferrari RA, Martins MD, Silva JA Jr, da Silva TD, Piovesan RF, Pavesi VC, Bussadori SK, Fernandes KP. Effects of low-level laser therapy on expression of TNF-α and TGF-β in skeletal muscle during the repair process. Lasers Med Sci 2011;26(3):335-340.
58. Assis L, Moretti AI, Abrahão TB, de Souza HP, Hamblin MR, Parizotto NA. Low-level laser therapy (808 nm) contributes to muscle regeneration and prevents fibrosis in rat tibialis anterior muscle after cryolesion. Lasers Med Sci 2013;28(3):947-955.
59. Yang WZ, Chen JY, Yu JT, Zhou LW. Effects of low power laser irradiation on intracellular calcium and histamine release in RBL-2H3 mast cells. Photochem Photobiol 2007;83(4):979–984.
60. Roth-Eichhorn S, Eberheim A, Bode HP, Gressner AM. Transformation-dependent calcium influx by voltage-operated calcium channels in stellate cells of rat liver. J Hepatol 1999;30:612–620.
61. Yu L, Lin Q, Liao H, Feng J, Dong X, Ye J. TGF-β1 induces podocyte injury through Smad3-ERK-NF-κB pathway and Fyn-dependent TRPC6 phosphorylation. Cell Physiol Biochem. 2010;26(6):869-878.
62. Harada M, Luo X, Qi XY, Tadevosyan A, Maguy A, Ordog B, Ledoux J, Kato T, Naud P, Voigt N, Shi Y, Kamiya K, Murohara T, Kodama I, Tardif JC, Schotten U, Van Wagoner DR, Dobrev D, Nattel S.Transient receptor potential canonical-3 channel-dependent fibroblast regulation in atrial fibrillation. Circulation 2012;126:2051–2064.
63. Davis J, Burr AR, Davis GF, Birnbaumer L, Molkentin JD. A TRPC6-dependent pathway for myofibroblast transdifferentiation and wound healing in vivo. Dev Cell 2012;23(4):705-715.
64. Saliba Y, Karam R, Smayra V, Aftimos G, Abramowitz J, Birnbaumer L, Farès N.Evidence of a Role for Fibroblast Transient Receptor Potential Canonical 3 Ca2+ Channel in Renal Fibrosis. J Am Soc Nephrol 2015;26(8):1855-1876.
65. Adapala RK, Thoppil RJ, Luther DJ, Paruchuri S, Meszaros JG, Chilian WM, Thodeti CK. TRPV4 channels mediate cardiac fibroblast differentiation by integrating mechanical and

soluble signals. J Mol Cell Cardiol 2013;54:45-52.

66. Venkatachalam K, Montell C. TRP channels. Annu Rev Biochem 2007;76:387-417.

67. Yang WH, Deng YT, Hsieh YP, Wu KJ, Kuo MY. NADPH Oxidase 4 Mediates TGFβ1-induced CCN2 in Gingival Fibroblasts. J Dent Res 2015;94(7):976-982.

68. Allen DG, Gervasio OL, Yeung EW, Whitehead NP. Calcium and the damage pathways in muscular dystrophy.Can J Physiol Pharmacol 2010;88(2):83-91.

69. Wuensch T, Thilo F, Krueger K, Scholze A, Ristow M, Tepel M. High glucose-induced oxidative stress increases transient receptor potential channel expression in human monocytes. Diabetes 2010;59(4):844-849.

TABLE 1. Laser specification

IRRADIATION PARAMETERS

Treated surface diameter (mm)	Modality	Distance from laser output (mm)	Irradiation time (s)
18	photoinductive	60	10
30	photoinductive	90	26

LASER BEAM PARAMETERS

Treated surface diameter (mm)	Laser type	*Wavelenght* (nm)	Irradiation mode	Power output (mW)	Target power (mW)	Laser beam diameter (mm)
18	Diode 635	635±5	continuous wave	89	89	18
30	Diode 635	635±5	continuous wave	89	89	30

LASER SPOT PARAMETERS

Treated surface diameter (mm)	Spot diameter /area at target level (mm/mm^2)	Power density (mW/cm^2)
18	18.6 / 273	32.6
30	30 / 703	12.6

SURFACE TREATMENT DATA

Treated surface diameter (mm)	Treated area (mm^2)	Treatment mode	Total energy delivered (mJ)	Total energy density (mJ/cm^2)
18	273	without contact	890	326
30	703	without contact	2314	329

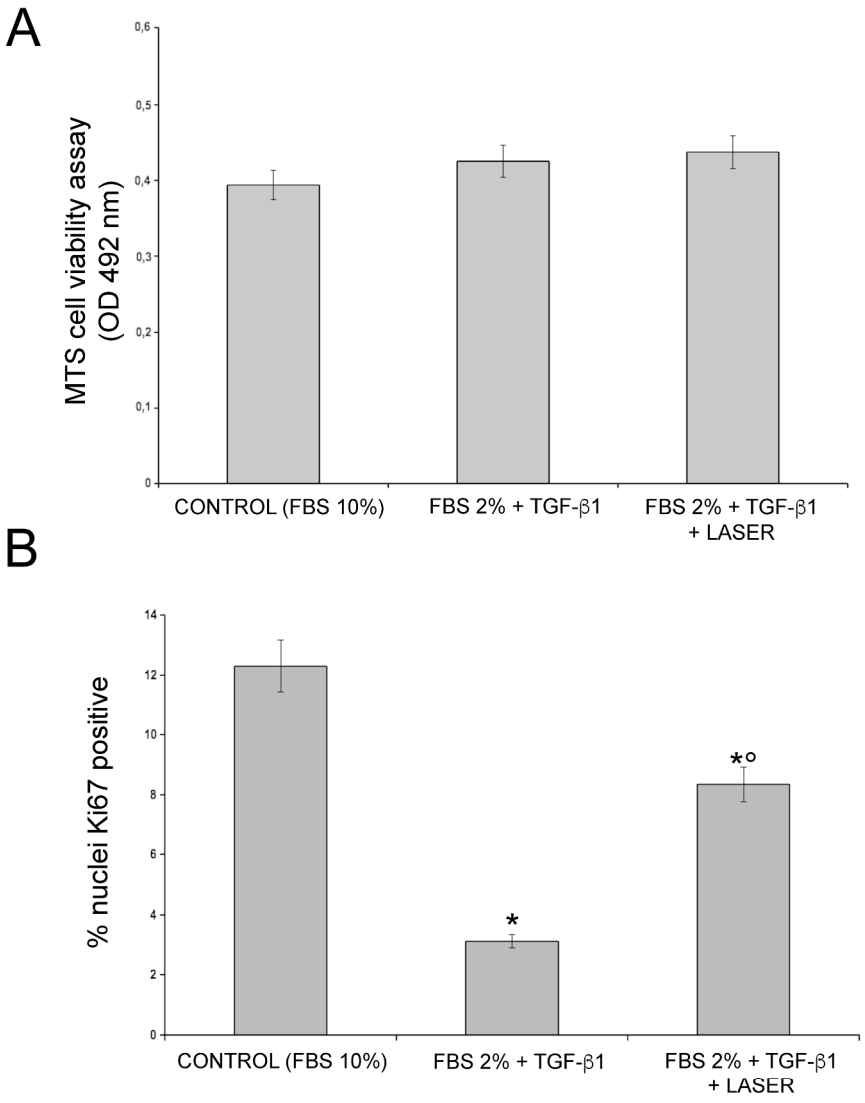

Figure 1

Effect of diode laser irradiation on viability and proliferation of TGF-β1 treated NIH/3T3 fibroblasts. The cells were cultured for 24 h in low serum (FBS 2%) in the presence of 2 ng/ml TGF-β1, irradiated or not with diode laser for 10 s or 26 s as reported in Table 1. Control cells were cultured in growth medium (FBS 10%). A) MTS cell viability assay. Otpical density of soluble colored formazan produced by MTS reduction, was evaluated using a multi-well scanning spectrophotometer at 492 nm. B) Evaluation of cell proliferation by confocal immunofluorescence analysis of Ki67 expression. The histogram shows the number of the cells with Ki67 positive nuclei expressed as percentage of the total nuclei number. Data shown are mean ± SEM and represent the results of at five independent experiments performed in triplicate. Significance of difference evaluated by one-way ANOVA and Newman–Keuls multiple comparison test: * $p < 0.05$ vs CONTROL (FBS 10%); ° $p < 0.05$ vs FBS 2% + TGF-β1.
241x325mm (300 x 300 DPI)

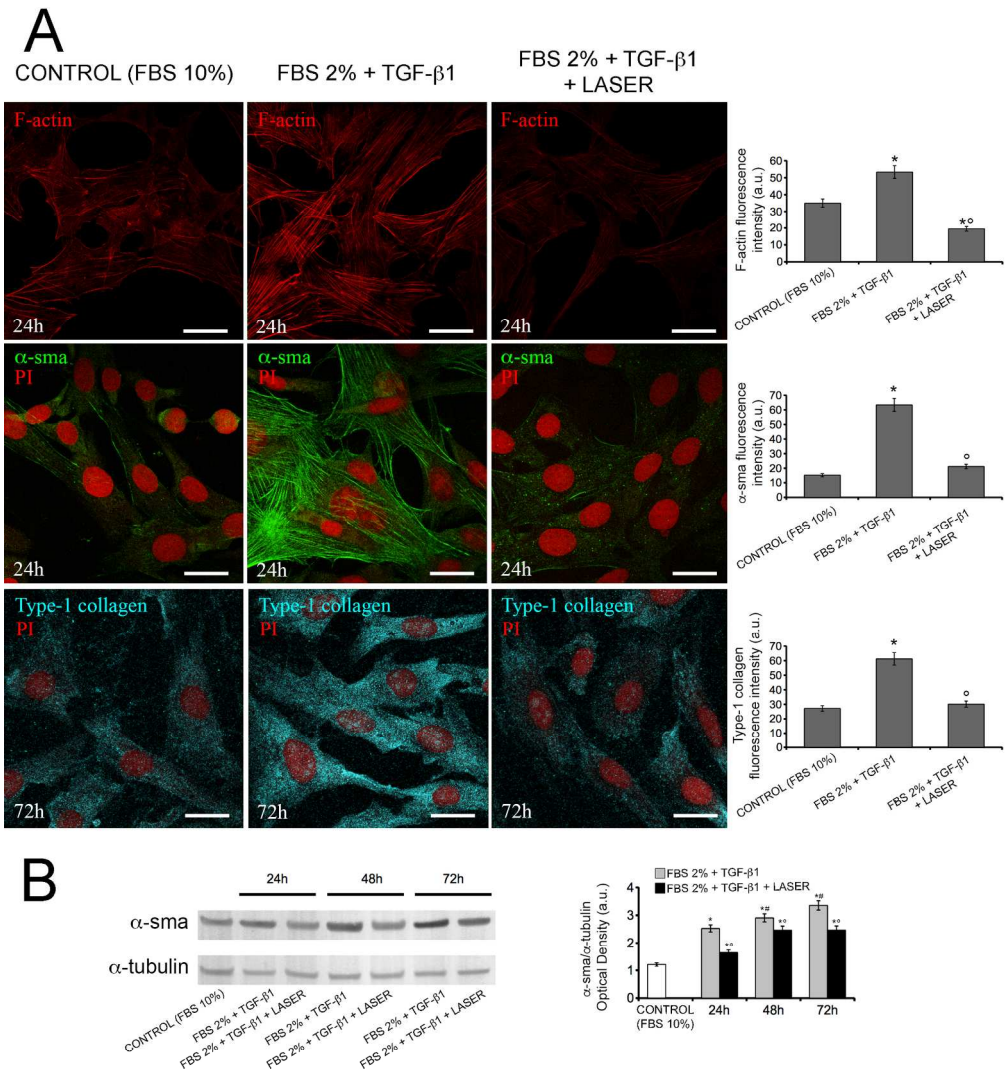

Figure 2

Effect of diode laser irradiation on fibroblast-myofibroblast transition. NIH/3T3 fibroblasts were cultured for 24 h, 48 h and 72 h in low serum (FBS 2%) in the presence of 2 ng/ml TGF-β1, irradiated or not with diode laser for 26 s as reported in Table 1 (treated surface diameter: 30 mm). Control cells were cultured in growth medium (FBS 10%). A) Representative confocal fluorescence images of the cells in the indicated experimental conditions, stained with TRITC-conjugated phalloidin to reveal F-actin (red) or immunostained with antibodies against α-sma (green) or type-1 collagen (cyan). Nuclei are counterstained in red with propidium iodide (PI). The histograms show the densitometric analyses of the intensity of the fluorescence signals for each specific marker performed on digitized images. Scale bar = 25 μm. B) Western blotting analysis of α-sma expression in fibroblasts in the indicated experimental conditions. The densitometric analysis of the bands normalized to α-tubulin is reported in the histogram. Data shown are mean ± SEM and represent the results of at least three independent experiments performed in triplicate. Significance of difference evaluated by one-way ANOVA and Newman–Keuls multiple comparison test: * p< 0.05 vs CONTROL (FBS 10%); ° p <0.05 vs FBS 2% + TGF-β1; # p <0.05 vs previous time.
205x235mm (300 x 300 DPI)

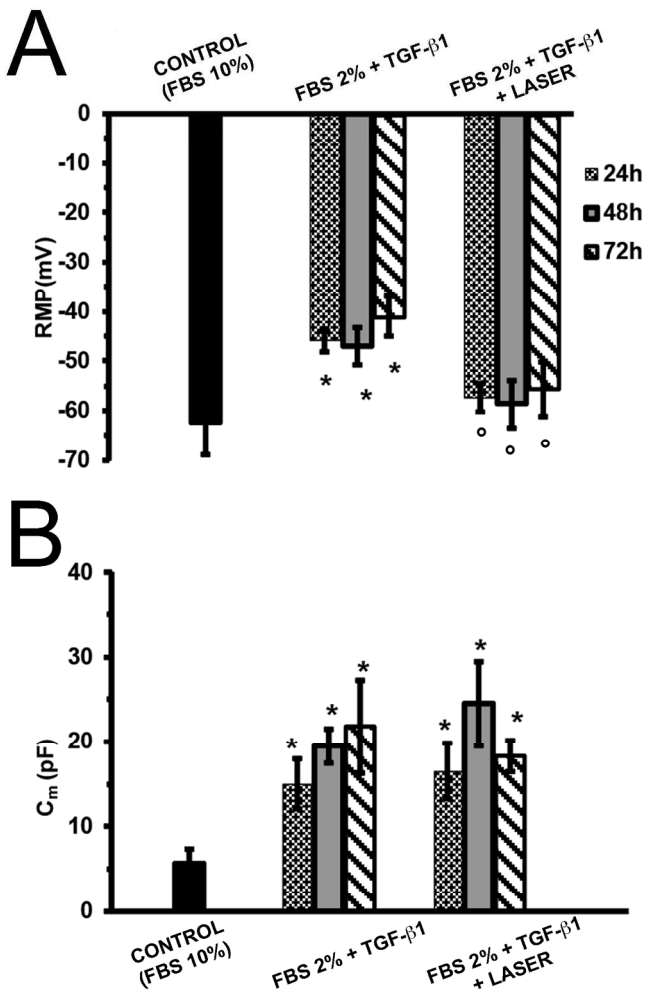

Figure 3

Effect of diode laser irradiation on electrophysiological plasmamembrane properties of TGF-β1 treated NIH/3T3 fibroblasts. NIH/3T3 fibroblasts were cultured for 24 h, 48 h and 72 h in low serum (FBS 2%) in the presence of 2 ng/ml TGF-β1, irradiated or not with diode laser for 26 s as reported in Table 1 (treated surface diameter: 30 mm). Control cells were cultured in growth medium (FBS 10%). A) Resting membrane potential (RMP) recorded by whole-cell patch-clamp technique in current clamp mode. B) Cell capacitance (Cm) commonly used as index of cell size, recorded by whole-cell patch-clamp technique in voltage clamp mode. Data are the mean ± SEM: CONTROL (FBS 10%), n = 20 cells; FBS 2% + TGF-β1, n = 30 cells; FBS 2% + TGF-β1 + LASER, n = 30 cells. Significance of difference evaluated by one-way ANOVA and Newman–Keuls multiple comparison test :* $p < 0.05$ vs CONTROL (FBS 10%); ° $p < 0.05$ vs FBS 2% + TGF-β1 treatment at the same time.
139x244mm (300 x 300 DPI)

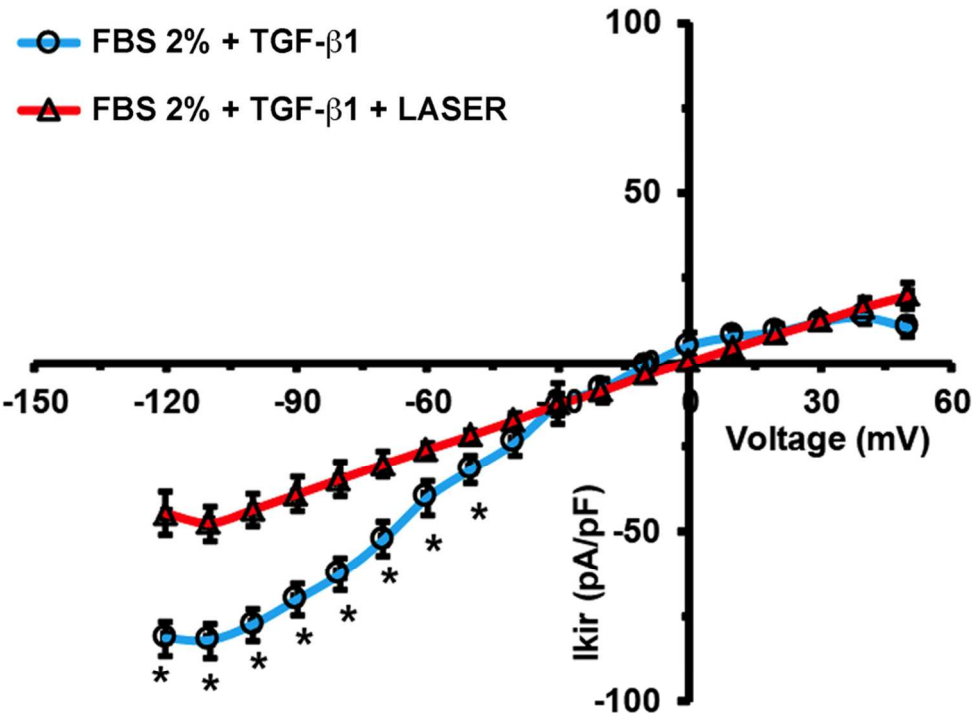

Figure 4

Effect of diode laser irradiation on delayed rectifier total outward K+ currents (IK,DR) on TGF-β1 treated NIH/3T3 fibroblasts.
I-V plot related to the inward rectifying K+ currents (IKir), obtained in response to ramp voltage pulse stimulation (HP = 0 mV) applied to fibroblasts cultured for 72 h in low serum (FBS 2%) in the presence of 2 ng/ml TGF-β1 (blue trace) and to TGF-β1 treated fibroblasts irradiated with the diode laser (red trace) for 26 s as reported in Table 1 (treated surface diameter: 30 mm). Each trace was obtained by pharmacological dissection in the presence of Kir channel blocker (Barium Chloride), subtracting the current recorded in the bath recording solution from that recorded in control solution. Current amplitude values were normalized for cell capacitance (Cm). Data are expressed as mean ± SEM (FBS 2% + TGF-β1, n = 22 cells; FBS 2% + TGF-β1 + LASER, n = 22 cells). Significance of difference evaluated by one-way ANOVA and Newman–Keuls multiple comparison test: * $p < 0.05$ vs FBS 2% + TGF-β1 + LASER.

90x101mm (300 x 300 DPI)

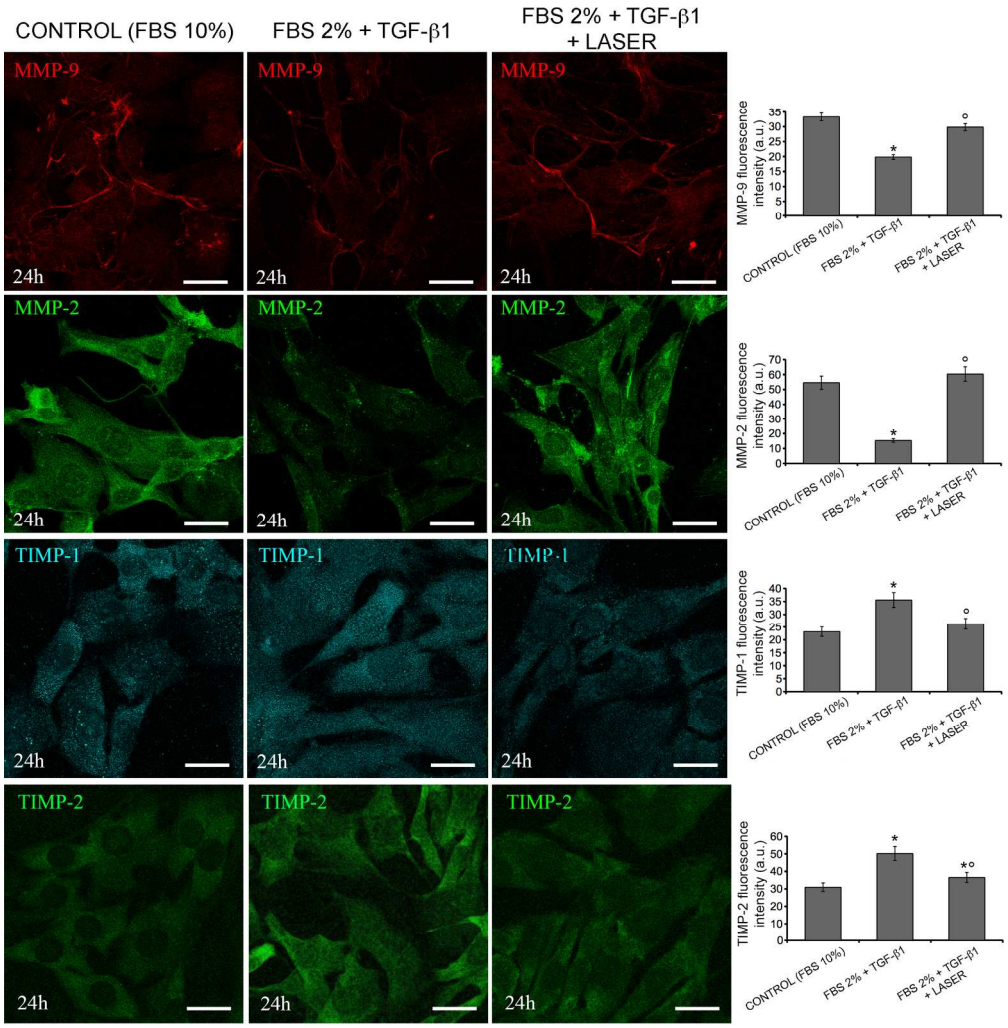

Figure 5

Effect of diode laser irradiation on MMP-2, MMP-9, TIMP-1 and TIMP-2 expression in TGF-β1 treated NIH/3T3 fibroblasts. Representative immunofluorescence confocal images of NIH/3T3 fibroblasts cultured in growth medium (CONTROL, FBS 10%) or cultured for 24 h in low serum medium (FBS 2%) in the presence of 2 ng/ml TGF-β1, irradiated or not with diode laser for 26 s as reported in Table 1 (treated surface diameter: 30 mm) and immunostained with antibodies against MMP-9 (red), MMP-2 (green), TIMP-1 (cyan) and TIMP-2 (green). Scale bar = 25 μm. Densitometric analyses of the intensity of the specific fluorescence signals performed on digitized images are reported in the histograms. Data shown are mean ± SEM and represent the results of at least three independent experiments performed in duplicate. Significance of difference evaluated by one-way ANOVA and Newman–Keuls multiple comparison test: * $p < 0.05$ vs CONTROL (FBS 10%); ° $p < 0.05$ vs FBS 2% + TGF-β1.
203x229mm (300 x 300 DPI)

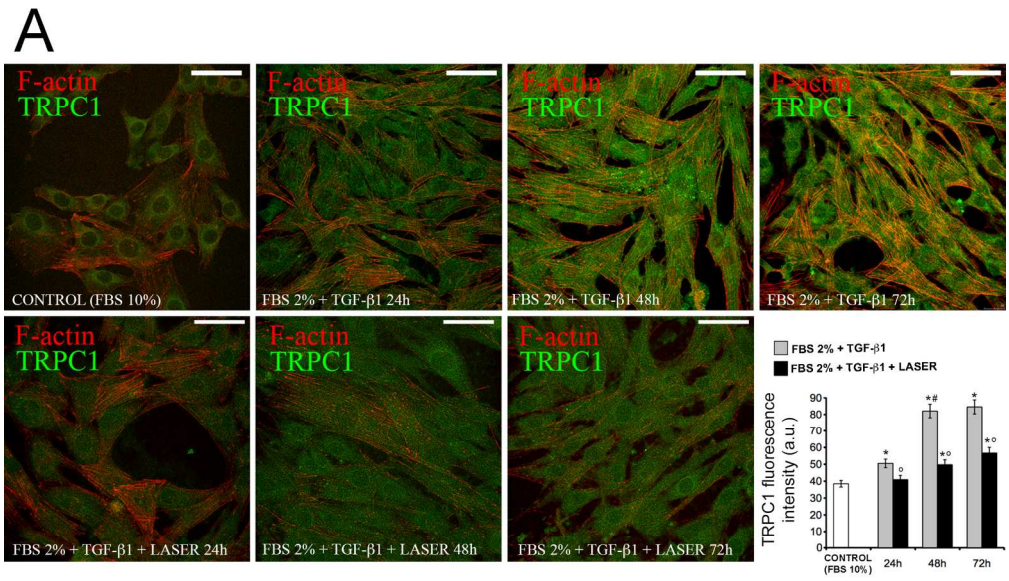

Figure 6

Effect of diode laser irradiation on TRPC1 expression and on currents through TRPC1 (ISAC) in TGF-β1 treated NIH/3T3 fibroblasts. NIH/3T3 fibroblasts were cultured for 24 h, 48 h and 72 h in low serum (FBS 2%) in the presence of 2 ng/ml TGF-β1, irradiated or not with diode laser for 26 s as reported in Table 1 (treated surface diameter: 30 mm). Control cells were cultured in growth medium (FBS 10%). A) Representative confocal fluorescence images of the cells in the indicated experimental conditions stained with TRITC-conjugated phalloidin to reveal F-actin (red) and immunostained with antibodies against TRPC1 (green). Scale bar = 50 μm. The histogram shows the densitometric analyses of the intensity of the TRPC1 fluorescence signal performed on digitized images. Data shown are mean ± SEM and represent the results of at least three independent experiments performed in triplicate. B) I-V plot related to the non selective cation currents fluxes through SACs (ISAC), obtained in response to ramp voltage pulse stimulation (HP = -40 mV) applied to fibroblasts cultured for 72 h in low serum (FBS 2%) in the presence of 2 ng/ml TGF-β1 not irradiated (green trace) or irradiated with diode laser (violet trace). Current amplitude is normalized for cell capacitance (Cm). Data are mean ± SEM (FBS 2% + TGF-β1, n = 20 cells; FBS 2% + TGF-β1 + LASER, n = 20 cells). Significance of difference evaluated by one-way ANOVA and Newman–Keuls multiple comparison

test. In A: * p< 0.05 vs CONTROL (FBS 10%); ° p < 0.05 vs FBS 2% + TGF-β1; # p < 0.05 vs previous time. In B * p < 0.05 vs FBS 2% + TGF-β1 + LASER.
212x250mm (300 x 300 DPI)

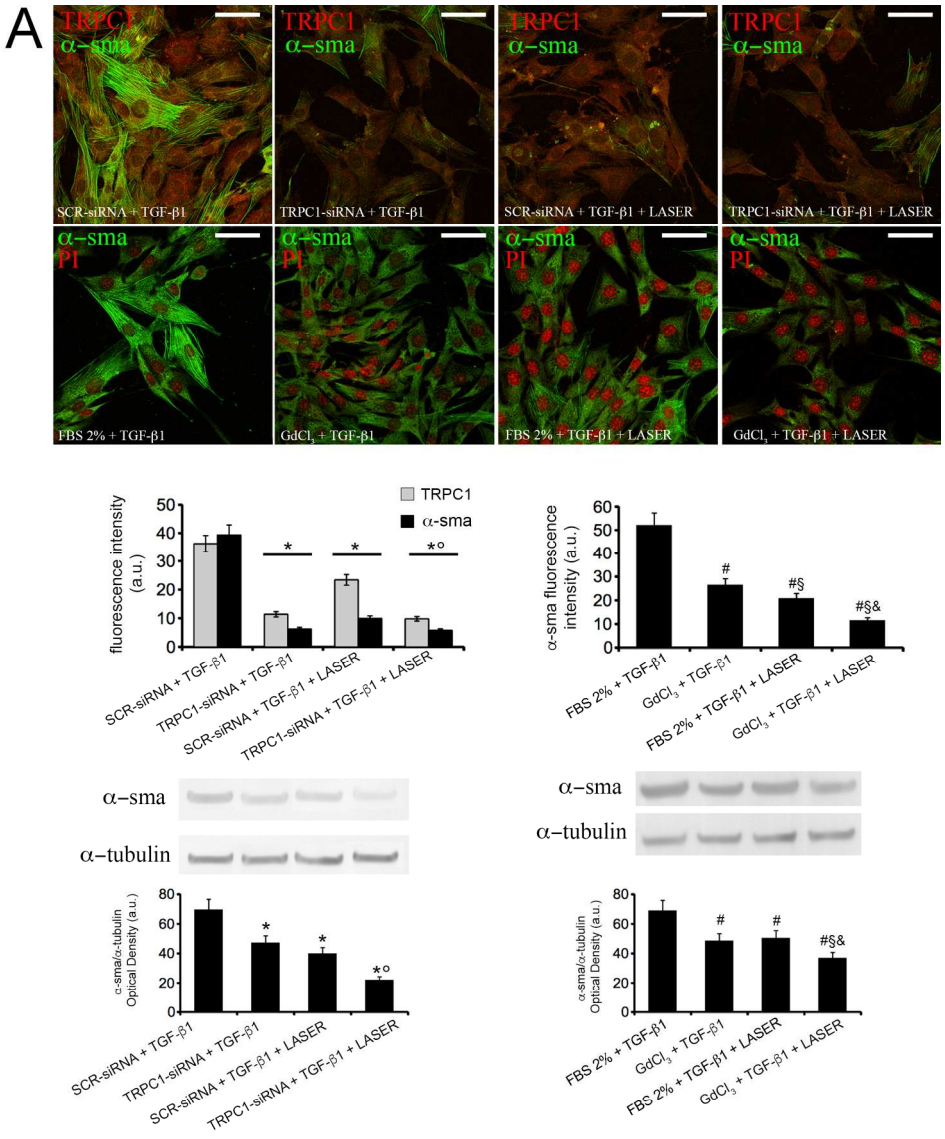

Figure 7

Effect of inhibition of TRPC1 expression and functionality on fibroblast-myofibroblast transition. To inhibit TRPC1 gene expression NIH/3T3 fibroblasts were silenced by specific TRPC1-siRNA cultured for 24 h in low serum (FBS 2%) in the presence of 2 ng/ml TGF-β1, irradiated or not with diode laser for 26 s as reported in Table 1 (treated surface diameter: 30 mm), SCR-siRNA was used as control. In other experiments the cells in low serum medium were pre-treated with Gadolinium Chloride (50 μM, GdCl3) a specific SAC channel blocker, before TGF-β1 addition and irradiation or not with diode laser. A) Representative confocal immuofluorescence images of the cells in the indicated experimental conditions immunostained with antibodies against TRPC1 (red, upper panel) and α-sma (green). Propidium iodide (PI, red) was used to counterstain nuclei. Scale bar = 50 μm. The histograms show the densitometric analyses of the intensity of the fluorescence signal for specific markers performed on digitized images. B) Western blotting analysis of α-sma expression in fibroblasts in the indicated experimental conditions. The densitometric analysis of the bands normalized to α-tubulin is reported in the histograms. Data shown are mean ± SEM and represent the results of at least three independent experiments performed in triplicate. Significance of difference

evaluated by one-way ANOVA and Newman–Keuls multiple comparison test: * p< 0.05 vs SCR-siRNA + TGF-β1; ° p < 0.05 vs SCR-siRNA + TGF-β1 + LASER; # p < 0.05 vs FBS 2% + TGF-β1; § p < 0.05 vs GdCl3 + TGF-β1; & p < 0.05 vs FBS 2% + TGF-β1 + LASER.
229x293mm (300 x 300 DPI)

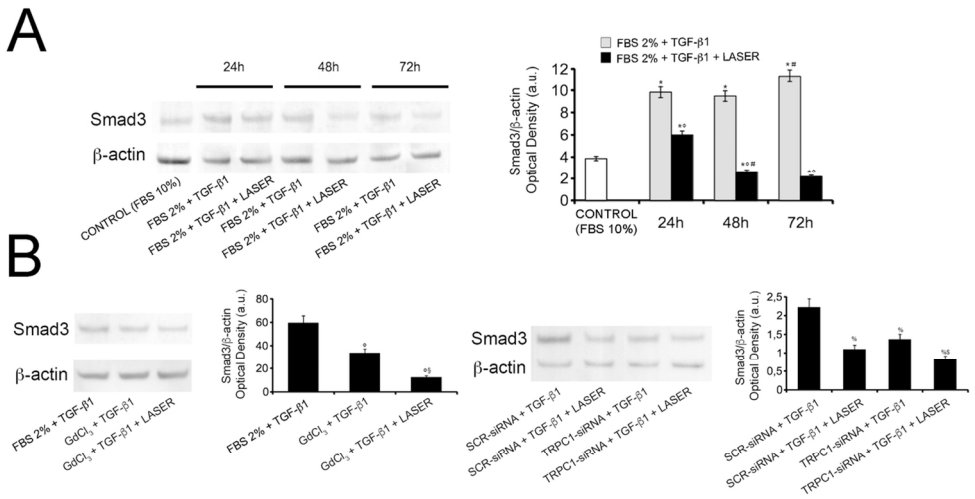

Figure 8

Effect of inhibition of TRPC1/SAC expression and functionality on TGF-β1/Smad3 signaling pathway. Western blotting analysis of Smad3 expression in NIH/3T3 fibroblasts A) cultured for 24 h, 48 h and 72 h in low serum (FBS 2%) in the presence of 2 ng/ml TGF-β1, irradiated or not with diode laser for 26 sec as reported in Table 1 (treated surface diameter: 30 mm) or in growth medium (CONTROL, FBS 10%); B) -left panel- cultured in low serum medium for 24 h, pre-treated with Gadolinium Chloride (50 μM, GdCl3) a specific SAC channel blocker, before TGF-β1 addition and irradiated or not with diode laser and -right panel- silenced for TRPC1 by specific TRPC1-siRNA and cultured for 24 h in low serum in the presence of TGF-β1 irradiated or not with diode laser. SCR-siRNa was used as control. The densitometric analyses of the bands normalized to β-actin are reported in the histograms. Data shown are mean ± SEM and represent the results of at least three independent experiments performed in triplicate. Significance of difference evaluated by one-way ANOVA and Newman–Keuls multiple comparison test: * $p < 0.05$ vs CONTROL (FBS 10%), ° $p < 0.05$ vs FBS2% + TGF-β1; # $p < 0.05$ vs previous time; § $p < 0.05$ vs GdCl3 + TGF-β1; % $p < 0.05$ vs SCR-siRNA + TGF-β1; $ $p < 0.05$ vs TRPC1-siRNA + TGF-β1.

117x77mm (300 x 300 DPI)